A refinement of the dickite structure and some remarks on polymorphism in kaolin minerals.[1]

By Robert E. Newnham, M.S., Ph.D.

Cavendish Laboratory, Cambridge University
and
Laboratory for Insulation Research, Massachusetts Institute of Technology, Cambridge, Massachusetts, U.S.A.

[Communicated by the Editor; taken as read 26 January 1961.]

Summary. The crystal structure of the clay mineral dickite ($Al_2Si_2H_4O_9$) has been refined to a greater accuracy than that reported in an earlier analysis. Improved lattice parameters are: a 5·150 ± 0·001, b 8·940 ± 0·001, c 14·424 ± 0·002 Å., β 96° 44′ ± 1′. The dickite structure shows several significant distortions from the geometry of the idealized kaolin layer, including deformation and rotation of the silica tetrahedra. The most striking features of the octahedral layer are the extremely short shared edges of 2·37 Å. Although the analysis was not sufficiently accurate to position the hydrogen atoms with certainty, a model consistent with the infra-red absorption spectra is proposed. The stacking sequences of kaolin-layer minerals have been considered with reference to the structural features observed in dickite. There are thirty-six ways of superposing two kaolin layers commensurate with the OH–O bonds found in kaolinite, dickite, and nacrite. The twelve sequences showing the least amount of cation–cation superposition between consecutive kaolin layers can be used to construct two one-layer cells, kaolinite and its mirror image, and twelve two-layer cells, including dickite and nacrite. The distortions of the kaolin layer introduce secondary variations in the interlayer bonding that suggest that dickite and nacrite are the most stable of the kaolin layer structures, since they possess the shortest oxygen–hydroxyl contacts.

THE basic structural unit of the kaolin-clay minerals is the kaolin layer. Its chemical constitution is given by the formula O_3-Si_2-$O_2(OH)$-Al_2-$(OH)_3$, which emphasizes the planar groupings of the structure. Each Si atom is tetrahedrally surrounded by three oxygens in the basal plane and a fourth in the layer above. The latter is shared with two aluminium ions, each of which is octahedrally co-ordinated to two oxygens and four hydroxyl groups, three in the uppermost layer and one coplanar with the apex oxygens. The Si tetrahedra share corners with three other tetrahedra, while each Al octahedron possesses three edges in common with other octahedra. Successive kaolin layers are held to each other only by van der Waals forces and long hydrogen

[1] Supported by the Nuffield Foundation, I.C.I. Ltd., and the U.S. Army Signal Corps, Office of Naval Research, and Air Force.

bonds. Various stacking sequences of the layers lead to several polymorphic structures: kaolinite, dickite, nacrite, and halloysite.

The present investigation is an extension of previous work (Newnham and Brindley, 1956) on the structure of dickite, the best crystallized of the kaolin minerals. A more precise analysis of the structure has been carried out using more experimental data and Fourier projections with less atomic overlap. The discussion of the structure emphasizes the distorted nature of the kaolin layer and its influence on the interlayer bonding and polymorphism problem.

Experimental.

The mineral used came from the Pine Knot colliery in Schuylkill County, Pennsylvania; chemical analysis (Honess and Williams, 1935) has shown this material to be of unusually high purity (46·14 wt. % SiO_2, 39·61 % Al_2O_3, and 13·91 % H_2O, which compares favourably with the theoretical composition: 46·55 % SiO_2, 39·49 % Al_2O_3, and 13·96 % H_2O). The present refinement was carried out on a small, plate-like specimen of dimensions $0{\cdot}20 \times 0{\cdot}08 \times 0{\cdot}04$ mm.

The lattice parameters of the dickite unit cell were redetermined from oscillation photographs taken about the a and b axes. The measurements were made on a modified Unicam oscillation camera (Farquhar and Lipson, 1946), in which the photographic film is mounted in the van Arkel position. Zero-layer-line reflections with θ near 90 degrees were measured using Cu-$K\alpha_1$ (λ = 1·54051 Å.) and Cu-$K\alpha_2$ (λ = 1·54433 Å.) radiation, and graphical extrapolation was used to eliminate the major systematic errors. A discussion of the method and the appropriate extrapolation formulae have been given by Weisz, Cochran, and Cole (1949). The results of the final graphical extrapolations are:

a 5·150±0·001, b 8·940±0·001, c 14·424±0·002 Å.

β 96° 44′±1′, V 659·6±0·3 Å^3., d_{002} 7·162±0·001 Å.

The axial ratio $a/b = 0{\cdot}5761 \pm 0{\cdot}0002$ differs by only 0·22 % from the 'ideal' ratio of $1/\sqrt{3}$. The space group of dickite is C_s^4—Cc with $4[Al_2Si_2O_5(OH)_4]$ per unit cell. The cell contains two kaolin layers related to one another by a c-glide symmetry plane and a stacking shift of $\Delta a/a = -0{\cdot}1642$, ideally $-1/6$.

The intensity data used in refining the atomic coordinates were collected about the [100]- and [110]-zone axes, employing a Weissenberg camera and Mo-$K\alpha$ radiation. Visual estimates were made of 420 reflections, about four times the number recorded in the previous investiga-

tion. No correction was made for absorption; its maximum effect on the intensity measurements was calculated to be less than 3 %.

The refinement was carried out by means of two-dimensional difference syntheses, beginning with the final coordinates of the earlier work. The structure-factor computations and Fourier syntheses were performed on EDSAC II using the scattering factors of Berghuis *et al.* (1955). Ten refinement cycles were calculated for both the (100) and (110) projections with small adjustments being applied to the atomic coordinates and temperature factors at the completion of each cycle. The initial coordinates gave an R factor of 20·2 %, which was reduced to 7·5 % for the coordinates given in table I. The interatomic distances and bond angles in table II were computed from the arithmetic mean of the (100) and (110) coordinates. The final structure factors listed in table III were calculated using the temperature factors $B_{\mathrm{Si}} = 0{\cdot}70$, $B_{\mathrm{Al}} = 0{\cdot}80$, and $B_{\mathrm{O}} = 1{\cdot}15$ Å^2. Electron-density maps calculated with the observed structure-factor amplitudes are shown in figs. 1*a* and 1*b*. Except for some juxtaposition in the basal oxygen layer (O_1, O_2, and O_3), the resolution of atoms in the two projections is excellent; one of the unsatisfactory features of the earlier analysis was the extensive overlap in the (010) projection.

The accuracy of the structure determination was assessed in three ways. The standard deviation of the coordinates was first estimated from the root-mean-square slope of the final difference maps, using the expression

$$\hat{\sigma}(x_n) = 2\{\overline{[\partial(\rho_o - \rho_c)/\partial x]}\}^{\frac{1}{2}}/C_n,$$

where ρ_o and ρ_c are the observed and calculated electron densities, and $C_n = \partial^2\rho_o/\partial x_n^2$, the central curvature of the nth atom evaluated from an F_o synthesis (method 1). Assuming $\sigma(F_o) = K|F_o|$, corroborating evidence for the experimental error was then obtained from

$$\hat{\sigma}(x_n) = \pi K\Big(\sum_{n=1}^{N} Z_n^2/2A\Big)^{\frac{1}{2}}/pZ_n,$$

in which Z_n is the atomic number, A the area of the projection, and p a function of the atomic shape (method 2). The constant K was taken as 0·1 following the suggestion of Lipson and Cochran (1953), who have described both methods in some detail. A third estimate of the error was obtained from the deviation of the three measurements of z (cf. table I) from their mean $\bar{z}$:

$$\hat{\sigma}(z_n) = c\Big[\sum_{i=1}^{3} (\bar{z}-z_i)^2\Big]^{\frac{1}{2}}/2 \text{ (method 3).}$$

TABLE I. Atomic coordinates in cell fractions.

	(100) projection		(110) projection*				Mean values		
Atom	y	z	x	y	z	z	x	y	z
Si_1	0·4006	0·0409	0·0117	0·3995	0·0406	0·0401	0·0117	0·4001	0·0405
Si_2	0·5733	0·0408	0·5002	0·5731	0·0402	0·0397	0·5002	0·5732	0·0402
Al_1	0·2520	0·2329	0·9154	0·2548	0·2314	0·2316	0·9154	0·2534	0·2320
Al_2	0·4175	0·2311	0·4190	0·4164	0·2301	0·2306	0·4190	0·4170	0·2306
O_1	0·2360	0·9940	0·9554	0·2385	0·9932	0·9946	0·9554	0·2373	0·9939
O_2	0·4708	0·9935	0·2587	0·4740	0·9956	0·9934	0·2587	0·4724	0·9942
O_3	0·5080	0·0068	0·7646	0·5130	0·0042	0·0064	0·7646	0·5105	0·0058
O_4	0·3889	0·1529	0·0803	0·3863	0·1512	0·1529	0·0803	0·3876	0·1523
O_5	0·5820	0·1522	0·5110	0·5805	0·1525	0·1530	0·5110	0·5813	0·1526
$(OH)_1$	0·2746	0·1579	0·5818	0·2769	0·1573	0·1569	0·5818	0·2758	0·1574
$(OH)_2$	0·2736	0·2962	0·2439	0·2729	0·2948	0·2935	0·2439	0·2733	0·2948
$(OH)_3$	0·3945	0·2988	0·7472	0·3953	0·2983	0·2973	0·7472	0·3949	0·2981
$(OH)_4$	0·5843	0·2965	0·3328	0·5820	0·2968	0·2955	0·3328	0·5832	0·2963

* Each atom appears twice in the (110) projection: at $(-x+y, z)$ and $(-x-y, z+\frac{1}{2})$.

TABLE II. Interatomic distances in Å. and bond angles in degrees.

Interatomic distances.

Silicon–oxygen, $\sigma = 0{\cdot}017$ Å.

Si_1–O_1	1·61	Si_2–O_1	1·63
Si_1–O_2	1·63	Si_2–O_2	1·62
Si_1O_3	1·63	Si_2–O_3	1·60
Si_1O_4	1·61	Si_2–O_5	1·62

Aluminium–oxygen, $\sigma = 0{\cdot}018$ Å.

Al_1–O_4	1·93	Al_2–O_4	1·98
Al_1–O_5	2·01	Al_2–O_5	1·94
Al_1–$(OH)_1$	1·93	Al_2–$(OH)_1$	1·90
Al_1–$(OH)_2$	1·83	Al_2–$(OH)_2$	1·88
Al_1–$(OH)_3$	1·86	Al_2–$(OH)_3$	1·86
Al_1–$(OH)_4$	1·86	Al_2–$(OH)_4$	1·85

Oxygen–oxygen, $\sigma = 0{\cdot}021$ Å.

Si_1 tetrahedron		Si_2 tetrahedron	
O_1–O_2	2·60	O_1–O_3	2·59
O_1–O_3	2·64	O_1–O_2	2·58
O_1–O_4	2·68	O_1–O_5	2·68
O_2–O_3	2·59	O_2–O_3	2·63
O_2–O_4	2·66	O_2–O_5	2·67
O_3–O_4	2·72	O_3–O_5	2·67
Al_1 octahedron		Al_2 octahedron	
O_4–O_5	2·76	O_4–O_5	2·81
O_4–$(OH)_1$	2·77	O_4–$(OH)_1$	2·76
O_4–$(OH)_2$	2·37*	O_4–$(OH)_2$	2·37*
O_4–$(OH)_3$	2·87	O_4–$(OH)_4$	2·90
O_5–$(OH)_1$	2·82	O_5–$(OH)_1$	2·76
O_5–$(OH)_2$	2·84	O_5–$(OH)_3$	2·84
O_5–$(OH)_4$	2·36*	O_5–$(OH)_4$	2·36*
$(OH)_1$–$(OH)_2$	2·36*	$(OH)_1$–$(OH)_3$	2·79
$(OH)_1$–$(OH)_4$	2·84	$(OH)_1$–$(OH)_3$	2·36*
$(OH)_2$–$(OH)_3$	2·79	$(OH)_3$–$(OH)_3$	2·80
$(OH)_2$–$(OH)_4$	2·72	$(OH)_3$–$(OH)_4$	2·81
$(OH)_3$–$(OH)_4$	2·82	$(OH)_3$–$(OH)_4$	2·72

* Shared edges.

Across vacant octahedral site

O_4–O_5	3·41	$(OH)_3$–$(OH)_3$	3·39
O_4–$(OH)_1$	3·47	$(OH)_3$–$(OH)_4$	3·47
O_5–$(OH)_1$	3·41	$(OH)_3$–$(OH)_4$	3·46

Interlayer distances

$(OH)_3$–O_1	2·94	$(OH)_4$–O_2	2·97
$(OH)_3$–O_3	3·12		

Interatomic angles.

Oxygen–silicon–oxygen, $\sigma = 0{\cdot}9°$

O_1–Si_1–O_2	106·9	O_1–Si_2–O_2	105·8
O_1–Si_1–O_3	109·2	O_1–Si_2–O_3	105·9
O_1–Si_1–O_4	111·8	O_1–Si_2–O_5	111·3
O_2–Si_1–O_3	104·9	O_2–Si_2–O_3	109·5
O_2–Si_1–O_4	110·1	O_2–Si_2–O_5	111·5
O_3–Si_1–O_4	113·8	O_3–Si_2–O_5	112·6

Silicon–oxygen–silicon, $\sigma = 1{\cdot}0°$

Si_1–O_1–Si_2	128·8	Si_1–O_3–Si_2	141·8
Si_1–O_2–Si_2	131·0		

Silicon–oxygen–aluminium, $\sigma = 0{\cdot}9°$

Si_1–O_4–Al_1	125·5	Si_2–O_5–Al_1	128·7
Si_1–O_4–Al_2	129·5	Si_2–O_5–Al_2	124·4

Oxygen–aluminium–oxygen, $\sigma = 0{\cdot}8°$

O_4–Al_1–O_5	89·0	O_4–Al_2–O_5	91·5
O_4–Al_1–$(OH)_1$	91·7	O_4–Al_2–$(OH)_1$	90·7
O_4–Al_1–$(OH)_2$	77·9	O_4–Al_2–$(OH)_2$	75·6
O_4–Al_1–$(OH)_3$	98·5	O_4–Al_2–$(OH)_3$	165·9
O_4–Al_1–$(OH)_4$	162·2	O_4–Al_2–$(OH)_4$	98·7
O_5–Al_1–$(OH)_1$	91·3	O_5–Al_2–$(OH)_1$	91·7
O_5–Al_1–$(OH)_2$	94·9	O_5–Al_2–$(OH)_2$	165·5
O_5–Al_1–$(OH)_3$	166·4	O_5–Al_2–$(OH)_3$	96·8
O_5–Al_1–$(OH)_4$	75·2	O_5–Al_2–$(OH)_4$	77·2
$(OH)_1$–Al_1–$(OH)_2$	168·0	$(OH)_1$–Al_2–$(OH)_2$	95·1
$(OH)_1$–Al_1–$(OH)_3$	77·1	$(OH)_1$–Al_2–$(OH)_3$	77·8
$(OH)_1$–Al_1–$(OH)_4$	97·0	$(OH)_1$–Al_2–$(OH)_4$	165·5
$(OH)_2$–Al_1–$(OH)_3$	97·9	$(OH)_2$–Al_2–$(OH)_3$	97·2
$(OH)_2$–Al_1–$(OH)_4$	94·8	$(OH)_2$–Al_2–$(OH)_4$	97·9
$(OH)_3$–Al_1–$(OH)_4$	98·7	$(OH)_3$–Al_2–$(OH)_4$	94·2

Aluminium–oxygen–aluminium, $\sigma = 0{\cdot}9°$

Al_1–O_4–Al_2	99·3	Al_1–$(OH)_3$–Al_2	106·9
Al_1–O_5–Al_2	99·1	Al_1–$(OH)_3$–Al_2	104·6
Al_1–$(OH)_1$–Al_2	100·5	Al_1–$(OH)_4$–Al_2	108·6

TABLE III. *Comparison of observed and calculated structure factors.*
(100) projection

k.	*l.*	*Fo.*	|*Fc.*|	*k.*	*l.*	*Fo.*	|*Fc.*|	*k.*	*l.*	*Fo.*	|*Fc.*|	*k.*	*l.*	*Fo.*	|*Fc.*|
0	0	*	52	4	7	24	26	8	4	11	10	12	8	4	4
	4	79	85		8	36	37		5	12	12		9	7	7
	6	42	40		9	23	24		6	8	8		10	14	14
	8	43	44		10	20	21		7	9	8		11	7	7
	10	32	37		11	7	5		8	12	11		12	9	8
	12	36	41		12	23	25		9	9	8		13	8	7
	14	24	27		13	9	9		10	8	7		14	7	7
	16	37	43		14	14	14		11	14	14		15	7	7
	18	10	9		15	4	3		12	11	11		16	13	10
	20	24	24		16	12	12		13<	4	4		17	8	7
	22	9	10		17	8	7		14	10	10		18<	4	3
	24	7	8		18	14	13		15	13	13		19	8	8
	26	18	16		19	6	6		16	5	4		20	6	6
	28	11	9		20<	4	4		17<	4	4		21	5	6
	30	7	5		21	5	6		18	4	6		22<	4	5
	32	6	5	6	0	76	79	10	0	12	11		23	4	5
2	0	18	16		1	13	13		1	12	12	14	0<	4	1
	1	32	30		2	33	33		2	7	8		1	4	4
	2	44	44		3	15	15		3	11	11		2<	4	2
	3	17	16		4	30	32		4	11	11		3<	4	3
	4	26	24		5	11	11		5	8	7		4<	4	3
	5	13	13		6	21	23		6	8	7		5	7	6
	6	20	21		7	14	14		7	20	20		6<	4	1
	7	5	6		8	16	16		8	18	17		7	6	5
	8	17	18		9	13	13		9	17	17		8<	4	4
	9	9	9		10	33	35		10	5	4		9<	4	2
	10	7	8		11	11	11		11	5	5		10<	4	1
	11	13	14		12	30	32		12	9	9		11	5	5
	12	13	14		13	9	9		13	5	6	16	0	4	3
	13	12	11		14	16	18		14<	4	2		1	9	7
	14	10	10		15	6	6		15	4	6		2<	4	1
	15	10	11		16	31	33		16	4	4		3	5	6
	16<	4	2		17	7	6		17	6	7		4<	4	2
	17	7	8		18	4	4		18<	4	5		5<	4	3
	18	10	9		19	5	6		19	12	10		6	4	3
	19<	4	3		20	19	17		20	5	5		7	13	10
	20	4	5		21<	4	3		21	4	3		8	5	5
	21<	4	4		22	5	7		22<	4	1		9	12	8
	22	5	5		23<	4	3		23	6	6		10	4	2
	23<	4	2		24	5	5	12	0	24	23	18	0<	4	4
	24	5	5		25<	4	2		1	15	13		1	9	6
4	0	7	5		26	13	11		2	7	8		2<	4	2
	1	7	6		27<	4	3		3	15	14		3	10	7
	2	14	12		28	7	6		4	17	16		4	5	5
	3	14	15	8	0	8	10		5	9	9		5<	4	5
	4	32	32		1	18	18		6	14	14		6<	4	5
	5	21	21		2	5	6		7	10	9		7	5	5
	6	10	9		3	9	8								

* Not observed.

TABLE III (*cont.*)

(110) projection ($h = -k'$, $k = k'$)

k'.	l.	$Fo.$	$\|Fc.\|$	k'.	l.	$Fo.$	$\|Fc.\|$	k'.	l.	$Fo.$	$\|Fc.\|$	k'.	l.	$Fo.$	$\|Fc.\|$
0	2	*	52	1	$\bar{13}$	10	10	3	0	8	7	4	0	16	14
	4	82	85		$\bar{14}$	7	7		1	77	79		1	20	18
	6	45	40		$\bar{15}$	10	10		2	6	7		2	11	11
	8	48	44		$\bar{16}$	11	12		3	42	42		3	14	14
	10	35	36		$\bar{17}$	12	12		4	7	7		4<	4	2
	12	40	41		$\bar{18}$<	4	1		5	27	28		5	6	6
	14	26	27		$\bar{19}$	8	8		6	6	6		6	16	16
	16	42	42		$\bar{20}$	7	7		7	30	31		7	10	8
	18	10	10		$\bar{21}$	8	9		8	8	8		8	12	11
	20	22	23		$\bar{22}$<	4	1		9	20	19		9	5	4
	22	9	11		$\bar{23}$	4	4		10	9	9		10	17	18
	24	9	8-	2	0	10	9		11	36	38		11	10	10
	26	14	16		1	8	7		12	9	8		12	17	18
	28	9	9		2	16	15		13	32	34		13	10	9
	30	4	5		3	5	5		14	8	8		14	11	11
1	0	32	32		4	25	23		15	16	15		15	8	6
	1	36	36		5	23	23		16	5	5		16	15	14
	2	23	22		6	20	20		17	32	32		17	8	8
	3	34	31		7	24	25		18	4	5		18	7	7
	4	21	19		8	39	39		19<	4	6		19<	4	2
	5	29	28		9	25	25		20	4	3		20	8	8
	6	4	3		10	17	16		21	14	13	4	$\bar{1}$	11	8
	7	11	11		11	10	11		22<	4	2		$\bar{2}$	8	7
	8	11	10		12	27	28		23	7	7		$\bar{3}$	7	6
	9	16	17		13	7	7		24<	4	1		$\bar{4}$	12	14
	10	6	7		14	15	15		25<	4	3		$\bar{5}$	7	7
	11	13	13		15<	4	4		26<	4	1		$\bar{6}$	14	15
	12	15	14		16	16	16		27	11	10		$\bar{7}$	4	3
	13<	4	4		17<	4	3		28<	4	1		$\bar{8}$	13	13
	14	11	11		18	10	9		29	10	8		$\bar{9}$	12	12
	15	12	13		19	9	8	3	$\bar{1}$	26	27		$\bar{10}$	17	19
	16	11	10		20<	4	4		$\bar{2}$	9	10		$\bar{11}$	7	7
	17	8	8		21	9	7		$\bar{3}$	35	38		$\bar{12}$	7	7
	18	4	5		22<	4	6		$\bar{4}$	6	6		$\bar{13}$	8	8
	19	10	10		23	7	6		$\bar{5}$	23	27		$\bar{14}$	10	12
	20	6	5	2	$\bar{1}$	6	5		$\bar{6}$	7	10		$\bar{15}$	5	7
	21	11	10		$\bar{2}$	13	14		$\bar{7}$	22	22		$\bar{16}$	8	8
	22<	4	4		$\bar{3}$	20	19		$\bar{8}$	6	6		$\bar{17}$<	4	2
	23<	4	4		$\bar{4}$	34	30		$\bar{9}$	37	41		$\bar{18}$	4	5
	24<	4	2		$\bar{5}$	22	24		$\bar{10}$<	4	5	5	0	4	3
	25	5	6		$\bar{6}$	23	23		$\bar{11}$	22	25		1	10	10
	26	4	5		$\bar{7}$	29	30		$\bar{12}$	4	2		2	10	9
	27	4	3		$\bar{8}$	26	27		$\bar{13}$	22	25		3	5	4
1	$\bar{1}$	48	47		$\bar{9}$	9	11		$\bar{14}$<	4	1		4	4	5
	$\bar{2}$	22	21		$\bar{10}$	24	24		$\bar{15}$	27	31		5<	4	3
	$\bar{3}$	22	20		$\bar{11}$	9	9		$\bar{16}$<	4	2		6	15	14
	$\bar{4}$	12	11		$\bar{12}$	18	19		$\bar{17}$<	4	2		7	12	11
	$\bar{5}$	25	24		$\bar{13}$<	4	3		$\bar{18}$<	4	5		8	16	15
	$\bar{6}$	11	9		$\bar{14}$	13	13		$\bar{19}$	12	16		9	15	14
	$\bar{7}$	12	12		$\bar{15}$	4	4		$\bar{20}$	4	3		10	19	19
	$\bar{8}$	9	7		$\bar{16}$	8	9		$\bar{21}$<	4	7		11<	4	1
	$\bar{9}$	10	10		$\bar{17}$	7	7		$\bar{22}$<	4	4		12<	4	5
	$\bar{10}$	12	12		$\bar{18}$	9	9		$\bar{23}$<	4	6		13	6	6
	$\bar{11}$	17	19		$\bar{19}$	9	8		$\bar{24}$<	4	3		14<	4	4
	$\bar{12}$	14	14		$\bar{20}$	7	7		$\bar{25}$	10	12		15<	4	2

* Not observed.

TABLE III (*cont.*)
(110) projection ($h = -k'$, $k = k'$)

k'.	l.	*Fo.*	$\|Fc.\|$	k'.	l.	*Fo.*	$\|Fc.\|$	k'.	l.	*Fo.*	$\|Fc.\|$	k'.	l.	*Fo.*	$\|Fc.\|$
5	16<	4	3	6	2	27	27	**6**	$\bar{7}$	4	4	**7**	$\bar{7}$	4	6
	17	8	7		3	9	7		$\bar{8}$	15	17	8	0<	4	2
	18<	4	0		4	16	15		$\bar{9}$	4	4		1<	4	2
	19<	4	5		5	9	8		$\bar{10}$	5	6		2<	4	3
	20<	4	4		6	15	14		$\bar{11}$<	4	4		3<	4	4
	21<	4	2		7	5	6		$\bar{12}$	10	10		4<	4	3
	22	10	9		8	19	20		$\bar{13}$<	4	4		5	4	2
5	$\bar{1}$	7	6		9	4	5		$\bar{14}$	12	12		6<	4	2
	$\bar{2}$	10	9		10<	4	1		$\bar{15}$	4	5		7	6	5
	$\bar{3}$	13	13		11<	4	5		$\bar{16}$<	4	1		8	4	2
	$\bar{4}$	16	16		12	15	14		$\bar{17}$<	4	6		9	7	5
	$\bar{5}$	5	5		13<	4	4		$\bar{18}$	8	10		10	9	6
	$\bar{6}$	22	22		14	10	11		$\bar{19}$<	4	3		11	10	8
	$\bar{7}$	12	13		15<	4	5		$\bar{20}$	4	5	8	$\bar{1}$<	4	3
	$\bar{8}$	5	6		16<	4	3	7	0<	4	1		$\bar{2}$<	4	4
	$\bar{9}$	6	6		17<	4	4		1	5	6		$\bar{3}$	6	7
	$\bar{10}$	7	8		18	11	11		2	4	5		$\bar{4}$<	4	3
	$\bar{11}$	7	8		19<	4	3		3	4	4		$\bar{5}$	10	9
	$\bar{12}$<	4	3		20<	4	7		4	5	5	9	0	4	4
	$\bar{13}$<	4	2		21<	4	3		5<	4	3		1<	4	2
	$\bar{14}$	7	7		22<	4	5		6<	4	3		2	4	4
	$\bar{15}$	5	4		23<	4	3		7	7	6		3	7	7
	$\bar{16}$	7	7		24	9	8		8	7	6		4	6	3
	$\bar{17}$	5	6	6	$\bar{1}$	7	8	7	$\bar{1}$<	4	3		5	4	4
	$\bar{18}$	6	6		$\bar{2}$	22	22		$\bar{2}$	4	4		6	4	4
	$\bar{19}$	6	6		$\bar{3}$	4	5		$\bar{3}$	7	7		7<	4	4
	$\bar{20}$	7	8		$\bar{4}$	12	14		$\bar{4}$	4	5		8	4	3
6	0<	4	4		$\bar{5}$	7	6		$\bar{5}$<	4	7		9	9	8
	1	7	8		$\bar{6}$	10	9		$\bar{6}$<	4	0	9	$\bar{1}$	11	9

The standard deviations of the coordinates are: method 1, Si 0·004 Å., Al 0·006 Å., O 0·013 Å.; method 2, Si 0·007 Å., Al 0·009 Å., O 0·015 Å.; method 3, Si 0·006 Å., Al 0·008 Å., O 0·010 Å., these results being averaged over the three crystallographic directions and over all atoms of the same element. The largest estimates of $\hat{\sigma}$, i.e. those of method 2, were applied in computing the standard deviations of the interatomic distances and bond angles given in table II. Differences in lengths or angles exceeding 2·3 σ were taken as significant in the discussion that follows.

Nature of the kaolin layer.

A single kaolin layer of the dickite structure is shown in fig. 2. There are two such layers in the unit cell, the second being related to the first by a *c*-glide symmetry plane. Within each kaolin layer, the silicon tetrahedral layer and the aluminium octahedral layer show considerable distortion from their idealized geometry, indicative of the strong interatomic forces exerted between them. Some of the deformation may be caused by the slight difference in natural size of the silica and alumina

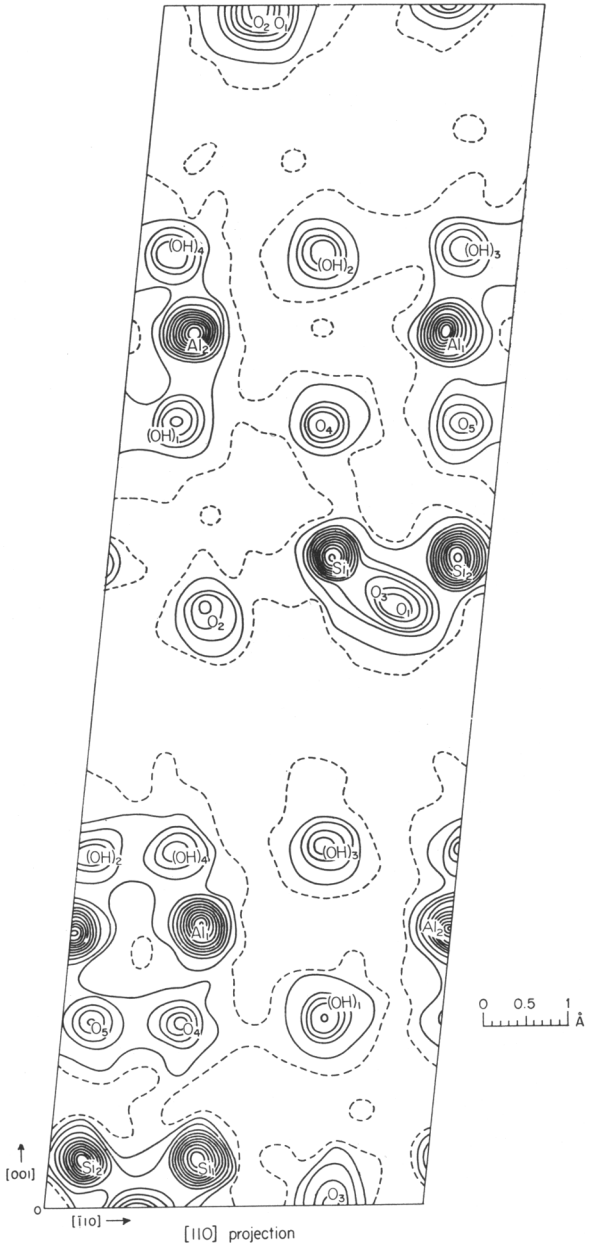

FIG. 1*a*. The [110] projection of the electron density in dickite, calculated with the observed structure amplitudes, $|Fo|$. Contours are drawn approximately at intervals of 2 electrons per Å^2.; the dashed contour is 1 electron per Å^2.

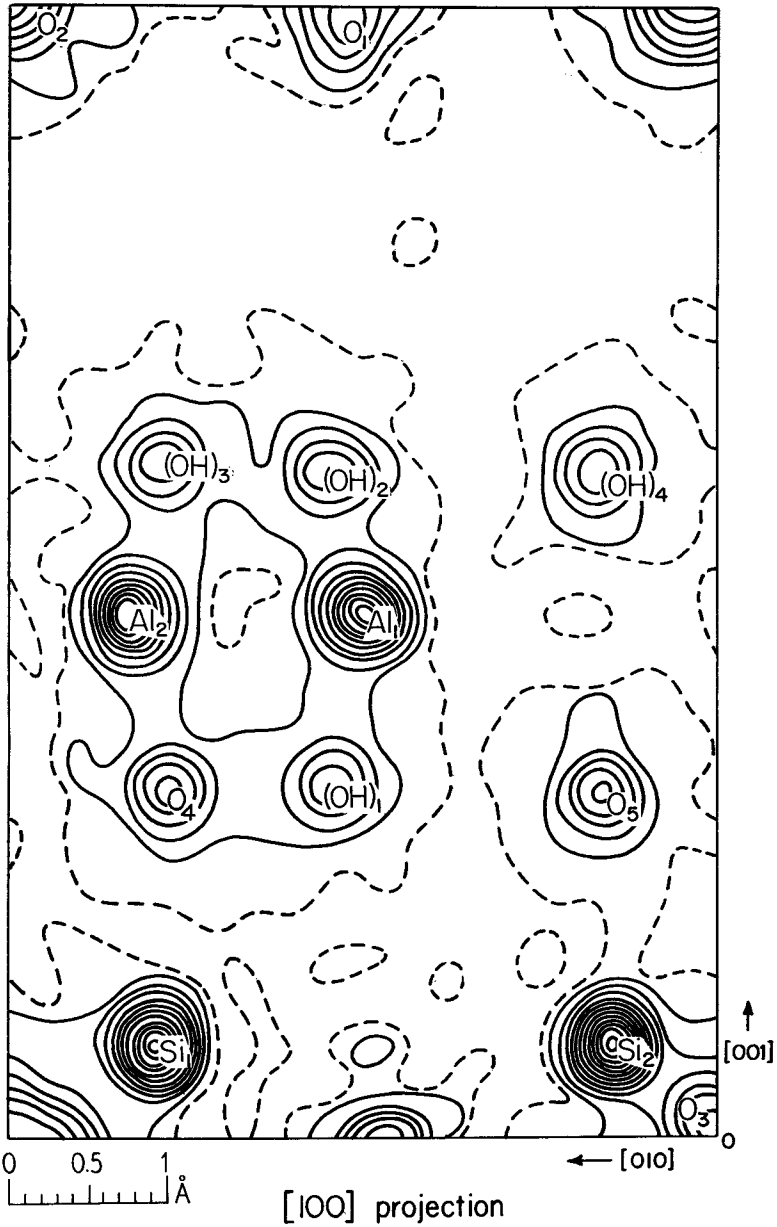

FIG. 1*b*. The [100] projection of the electron density in dickite. Details as in fig. 1*a*.

layers; the Al octahedral layer, as found in gibbsite for example, is somewhat smaller than a Si_2O_5 sheet with Si–O distances of 1·6 Å. Such a misfit would lead to tension in the octahedral layer and compression of the silica sheet. The resulting influence on the morphology of various layer-lattice silicates has been discussed by Bates (1959).

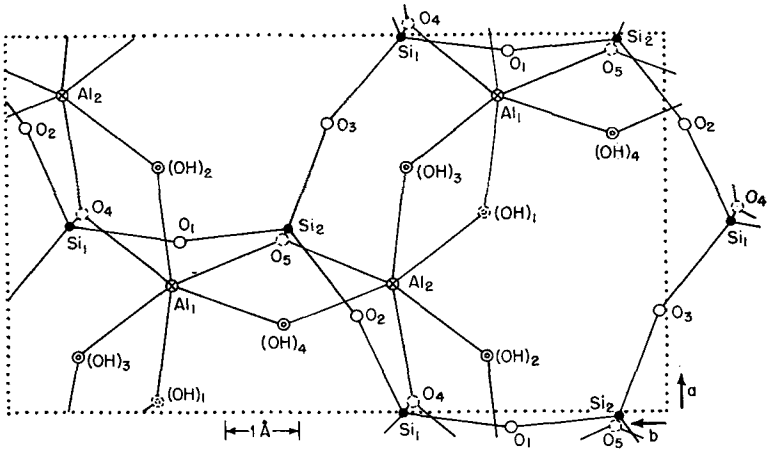

FIG. 2. A portion of the dickite kaolin-layer.

The silica layer is compressed through rotation of the tetraheda in (001). The Si_1 and Si_2 tetrahedra are rotated in opposite directions by about 7·5° with the directions of rotation apparently determined by the attractive force between Al_1 and O_1 and between Al_2 and O_2. Further evidence of compression in the silica layer is given by the observed deformation of individual tetrahedra. The O–O distances and O–Si–O bond angles show that the tetrahedra are contracted in the oxygen basal plane and elongated along c^*, normal to the basal plane. All distances and angles that involve the apex oxygens O_4 and O_5 are larger than those that do not. Despite this deformation, none of the silicon–oxygen bond lengths differ significantly from their arithmetic mean of 1·62 Å., slightly larger than the value $1{\cdot}60 \pm 0{\cdot}01$ recommended by Smith (1954). Recent refinements of coesite (Zoltai and Buerger, 1959) and danburite (Johannson, 1959) also show mean Si–O distances of 1·62 Å. Another feature of the silica sheet is the puckering in the basal oxygen plane. Atom O_3 is approximately 0·17 Å. higher than O_1 and O_2, thus causing corrugations running along [110] and [1$\bar{1}$0] in alternate kaolin layers. These corrugations arise as a result of the

shortened shared edges in the Al octahedral layer. Oxygens O_4 and O_5 are shifted toward $(OH)_2$ and $(OH)_4$, respectively, causing the silica tetrahedra to be tilted in such a way as to depress O_1 and O_2 while elevating O_3.

The distortions in the Al layer are best illustrated by the three classes of oxygen–oxygen distances: the six O–O distances across the vacant octahedral site ranging between 3·39 and 3·47 Å. (mean 3·43 Å.), the eighteen unshared octahedral edges from 2·72 to 2·90 Å. (mean 2·80 Å.), and the three shared octahedral edges of 2·37 Å. All twenty-seven distances would be equal if the octahedra were undistorted. The short shared edges are particularly striking since they are 0·1 Å. less than those observed in comparable structures. The shortest O–O distances found in gibbsite (Megaw, 1934) and diaspore (Busing and Levy, 1958) are 2·47 and 2·46 Å., respectively. The shortened shared edges arise as a consequence of the expansion of the Al–O,OH network and also exert a marked influence on the O–Al–O bond angles; those that subtend shared edges are about 20° smaller than the others. The aluminium ions are not equidistant from their nearest neighbours; the $Al–(OH)_{2,3,4}$ distances average 1·86 Å., while those to the O,OH layer have a mean of 1·95 Å. The irregular configurations and interatomic distances are very similar to those found in diaspore by Busing and Levy (1958). The Al atoms in dickite are closer to the hydroxyl layer than to the O,OH layer because of the repulsive forces originating from the Si ions. The effect is enhanced by the stretching forces acting on the octahedra, allowing greater freedom of motion for the aluminium cations. Al_2 is slightly lower than Al_1 since it lies directly beneath a silicon ion in the layer above.

Hydrogen positions and interlayer bonding.

The contacts between kaolin layers illustrated in fig. 3 show the hydroxyls and oxygens linked together in pairs. The $(OH)_2–O_1$ and $(OH)_4–O_2$ distances are 2·94 and 2·97 Å., respectively, while $(OH)_3–O_3$ is a significantly longer bond of 3·12 Å. because of the puckering of the oxygen layer. All other interlayer oxygen–oxygen distances are greater than 3·5 Å. The rotation directions of the silica tetrahedra act to reduce the length of the OH–O contacts. If the hydroxyls of one layer are rotated clockwise because of the shortened shared edges, then the oxygens of the adjacent kaolin layer also undergo a clockwise movement. This mechanism appears to be important in regard to polymorphism in kaolin minerals and will be discussed further in the next section.

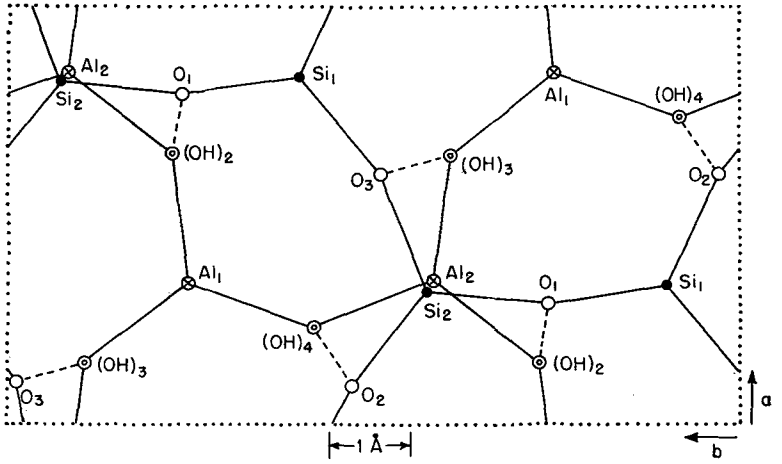

FIG. 3. Dickite interlayer bonding.

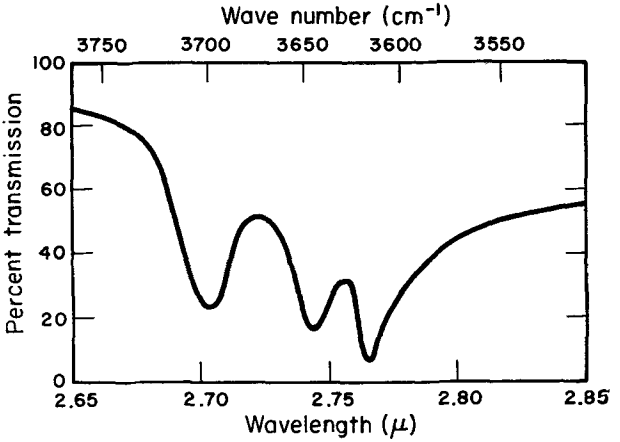

FIG. 4. Infra-red spectrograms of Schuylkill dickite.

The structure analysis was not sufficiently accurate to fix the hydrogen positions. In a survey of hydrogen-bearing compounds, McDonald (1956) has shown that the peak heights of hydrogen atoms range from 0·7 to 1·0 electrons per Å^2. An F_o or (F_o-F_c) synthesis for non-centrosymmetric dickite might therefore be expected to show maxima of 0·5 electrons per Å^2. at the hydrogen positions. Unfortunately such detail was obscured by spurious background; the final F_o projections (figs. 1*a* and 1*b*) gave a standard deviation in the electron density of 0·3 elec-

trons per Å^2. There are, however, small maxima in the interlayer region which are suggestive of hydrogen atoms. A three-dimensional analysis, with counter data for the low-angle reflections, is probably necessary to resolve the question.

Less ambiguous information regarding the disposition of the hydrogen atoms was obtained from the OH–O infra-red vibration spectra of Schuylkill dickite. The mineral was prepared as a mull in high-boiling paraffin (Nujol) and 'Perfluorolube' and mounted between glass cover

TABLE IV. Infra-red absorption data for Schuylkill dickite.

Wavelength (μ)	Wave number (cm.$^{-1}$)	Relative intensity	Proposed structure	O–O distance (Å.)
$2{\cdot}70_3$	370_0	medium	$(O–H)_1$	—
$2{\cdot}74_4$	364_4	medium	$(O–H)_3—O_3$	3·12
$2{\cdot}76_5$	361_7	strong	$(O–H)_2—O_1$ $(O–H)_4—O_2$	2·97 2·94

slides. Microscopic examination showed that most of the dickite crystals were oriented parallel to (001), despite extensive grinding. Excellent resolution of the important absorption bands near 3 700 cm.$^{-1}$ (fig. 4) was obtained with a Beckman DK-1 instrument, employing a quartz optical system. The wave-lengths of the dickite absorption spectra listed in table IV were calibrated with the polyethylene absorption band at 3·508 μ. It is unlikely that any of the dickite bands are due to adsorbed water since identical results were obtained with specimens heated at 400° C. In a previous investigation (Adler *et al.*, 1950) of dickite from St. George, Utah, U.S.A., and San Juanita, Mexico, infra-red absorption spectra were found at 2·73, 2·83, and 3·33 μ.

Tentative structural assignments for the OH–O stretching frequencies are proposed in table IV. The choices are somewhat arbitrary but are based on the survey of Nakamoto *et al.* (1955), in which the infra-red vibration frequencies of a large number of hydrogen-bonded compounds have been correlated with pertinent interatomic distances. The proposed model places the hydrogen atoms of $(OH)_2$, $(OH)_3$, and $(OH)_4$ on long hydrogen bonds that connect the hydroxyl groups to their closest oxygen neighbours in the adjacent kaolin layer, while $(OH)_1$ functions primarily as a free hydroxyl group.

Polymorphism in kaolin minerals.

Three polymorphic forms of kaolin-layer silicates are found in nature: kaolinite, dickite, and nacrite. In addition to these crystalline varieties, there are a number of minerals showing a more or less irregular sequence

of kaolin layers. As pointed out by Hendricks (1938), the key feature of the interlayer coordination is the manner in which oxygens and hydroxyls approach one another in pairs to form long hydrogen bonds. The type of stacking translations that leads to the required interlayer bonding (table V) was determined by Brindley (1951). His analysis gives an adequate account of the possible one-layer structures, but it cannot be applied to multi-layer unit cells in which consecutive kaolin layers are rotated with respect to one another.

TABLE V. Translations of the base-centred unit cell leading to paired oxygen-hydroxyl bonds (after Brindley, 1951). The numbers refer to the stacking sequences of table VI and fig. 8.

		$\Delta b/b$.						
		$-\frac{1}{2}$.	$-\frac{1}{3}$.	$-\frac{1}{6}$.	0.	$+\frac{1}{6}$.	$+\frac{1}{3}$.	$+\frac{1}{2}$.
	$-\frac{1}{2}$	1	—	31	—	19	—	1
	$-\frac{1}{3}$	—	13	—	7	—	25	—
	$-\frac{1}{6}$	—	—	—	—	—	—	—
$\Delta a/a$	−0	—	19	—	1	—	31	—
	$+\frac{1}{6}$	7	—	25	—	13	—	7
	$+\frac{1}{3}$	—	—	—	—	—	—	—
	$+\frac{1}{2}$	1	—	31	—	19	—	1

In order to determine all the permissible stacking sequences for two kaolin layers, the primitive unit cell shown in fig. 5 was chosen as a reference. The six different ways in which the oxygens of the next kaolin layer can be paired with the hydroxyls of the reference cell are illustrated in fig. 6. For each of the six possibilities there are six ways to construct the second kaolin layer; these are related to one another by a rotation angle ϕ (fig. 7). Thus there are $6 \times 6 = 36$ different superposition patterns for two kaolin layers. The situation is somewhat more complex than that of the mica family (Smith and Yoder, 1956), where there are only six different stacking sequences. Fig. 8 shows the thirty-six permissible second layers for the reference cell of fig. 5; their stacking shifts and rotation angles are given in table VI. Six of these sequences (for which $\phi = 0$) are identical with those proposed by Brindley (cf. table V). Interlayer shifts related by unit-cell translations or the C-face centring operation are of course identical.

In constructing a unit cell of n kaolin layers from the permitted stacking sequences, the reference axes in the nth layer must maintain the same orientation as those in the origin layer. In other words, $\phi_1+\phi_2+ \ldots +\phi_n = 2\pi N$, where N is an integer. For a one-layer cell, only those sequences that have $\phi = 0$ need be considered; in two-layer cells such as dickite, $\phi_1+\phi_2 = 0$ or 2π. With the thirty-six stacking sequences of

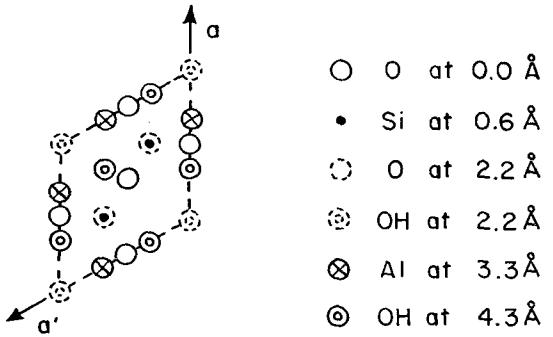

FIG. 5. Primitive reference cell.

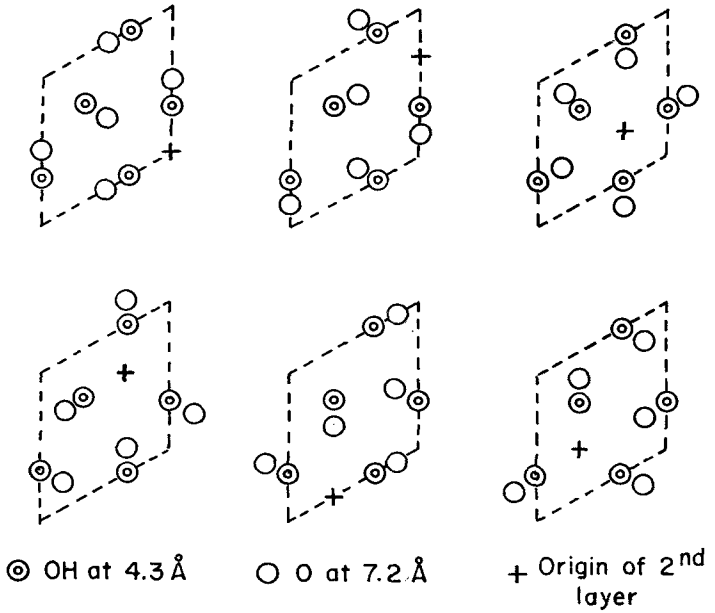

FIG. 6. Six ways of placing the oxygen layer over the hydroxyl layer.

table VI, six one-layer and 108 two-layer unit cells can be constructed. The discussion that follows attempts to justify nature's preference for only a small group of these polymorphic varieties. This objective can be accomplished with the following assumptions concerning the most stable configurations: the highly charged Si^{4+} and Al^{3+} cations tend to avoid one another as much as possible; oxygens and hydroxyls approach one another as close as possible to promote strong interlayer bonding.

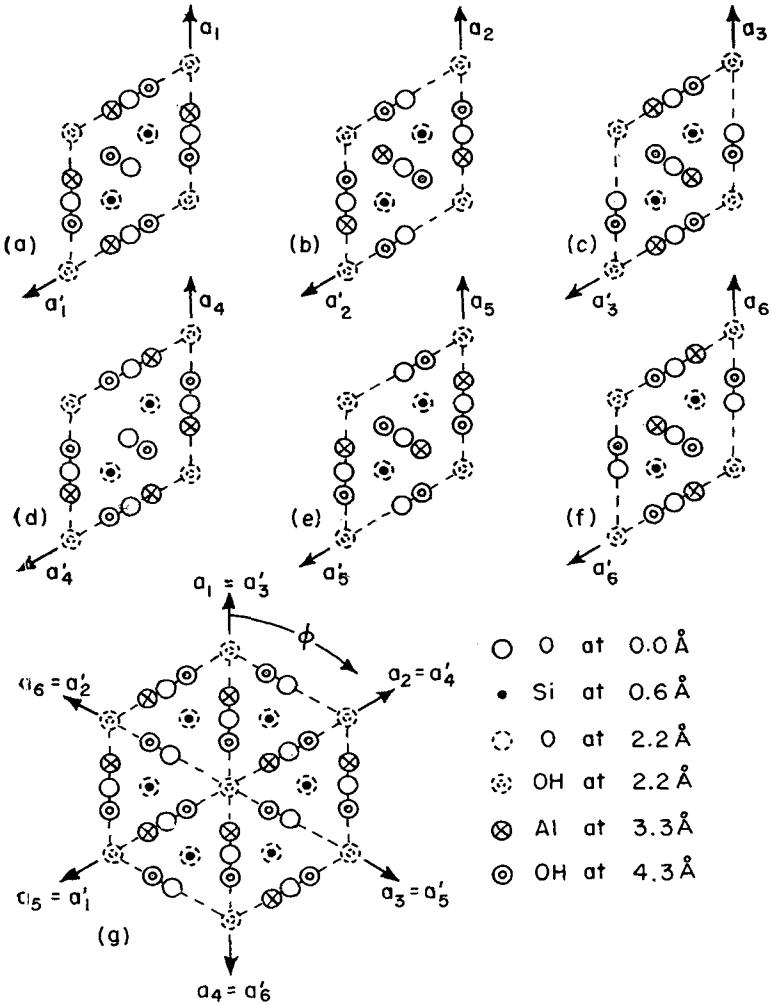

FIG. 7. The six methods, (*a*)–(*f*), of constructing a kaolin layer from a given basal oxygen network; (*g*) shows how the cells can be related by a rotation angle ϕ.

The first of these assumptions reduces the contribution of the cations to the Coulomb energy of the crystal; it can be applied to the stacking sequences of table VI by eliminating those with the greatest amount of cation–cation superposition in consecutive layers. The superimposed cations are enumerated in table VI, from which it can be seen that at least one-fourth of the second-layer cations are vertically coincident

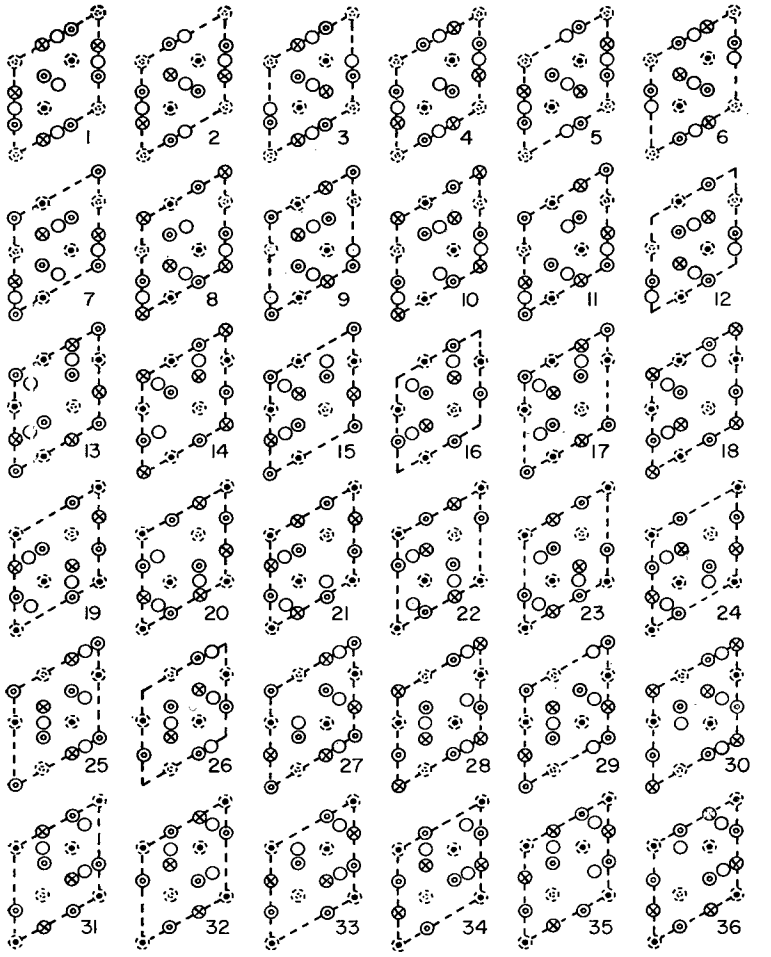

FIG. 8. Thirty-six possible second layers for the reference cell in fig. 5.

with those of the reference cell. If the stacking arrangements showing more than the minimum amount of overlap are rejected as energetically unfavourable, the following twelve remain: 7, 9, 11, 20, 22, 24, 25, 27, 29, 32, 34, and 36. The two one-layer and twelve two-layer cells that can be constructed from these stacking sequences are given in table VII.

The two single-layer cells are those of kaolinite and its mirror image, perhaps more properly designated as right- and left-handed kaolinite. The

TABLE VI. The thirty-six stacking sequences and their relationship with the reference cell.

No.	Interlayer shift and rotation angle Δa	$\Delta a'$	ϕ	Cation superposition Si_{II}–Si_I	Si_{II}–Al_I	Al_{II}–Si_I	Al_{II}–Al_I	Oxygen–hydroxyl approach Rotation	Pucker
1	0	0	0	1	0	0	1	U	F
2			1	1	0	0	0	F	U
3			2	1	0	0	½	U	U
4			3	1	0	0	0	F	F
5			4	1	0	0	½	U	U
6			5	1	0	0	0	F	U
7	⅔	0	0	0	½	0	0	F	U
8			1	0	½	½	0	U	F
9			2	0	½	0	0	F	U
10			3	0	½	½	0	U	U
11			4	0	½	0	0	F	F
12			5	0	½	1	0	U	U
13	⅓	⅓	0	0	1	0	0	F	F
14			1	0	1	½	0	U	U
15			2	0	1	0	0	F	U
16			3	0	1	1	0	U	F
17			4	0	1	0	0	F	U
18			5	0	1	½	0	U	U
19	⅔	⅓	0	½	0	0	½	U	U
20			1	½	0	0	0	F	F
21			2	½	0	0	1	U	U
22			3	½	0	0	0	F	U
23			4	½	0	0	½	U	F
24			5	½	0	0	0	F	U
25	0	⅔	0	0	½	0	0	F	U
26			1	0	½	1	0	U	U
27			2	0	½	0	0	F	F
28			3	0	½	½	0	U	U
29			4	0	½	0	0	F	U
30			5	0	½	½	0	U	F
31	⅓	⅔	0	½	0	0	½	U	U
32			1	½	0	0	0	F	U
33			2	½	0	0	½	U	F
34			3	½	0	0	0	F	U
35			4	½	0	0	1	U	U
36			5	½	0	0	0	F	F

Key: The interlayer translations are referred to the primitive unit cell of fig. 5, and the angle ϕ is expressed in multiples of $\pi/3$ radians. In the cation superposition columns, the digit '1' denotes complete coincidence of the cations in the second layer (II) over those of the reference cell (I). '½' and '0' mean that half or none of the cations are superimposed. Distortions that lead to close OH–O distances for a certain stacking sequence are denoted with an 'F' in the final two columns; 'U' signifies an unfavourable distortion.

relationship between these two structures, which contain stacking sequences 7 and 25 respectively, is shown in fig. 9. Kaolinite belongs to

TABLE VII. One- and two-layer unit cells formed from the stacking sequences with minimum cation superposition.

One-layer structures.	
7, 7, 7, 7, 7, . . .	25, 25, 25, 25, 25, . . .
Two-layer structures.	
7, 25, 7, 25, 7, . . .	22, 22, 22, 22, 22, . . .
34, 34, 34, 34, 34, . . .	22, 34, 22, 34, 22, . . .
9, 11, 9, 11, 9, . . .	9, 29, 9, 29, 9, . . .
11, 27, 11, 27, 11, . . .	27, 29, 27, 29, 27, . . .
20, 24, 20, 24, 20, . . .	20, 36, 20, 36, 20, . . .
24, 32, 24, 32, 24, . . .	32, 36, 32, 36, 32, . . .

the acentric triclinic point group 1, and may therefore show enantiomorphism (cf., for example, Henry *et al.* (1951)). In their analysis of the structure, Brindley and Robinson (1946*a*) chose the right-handed struc-

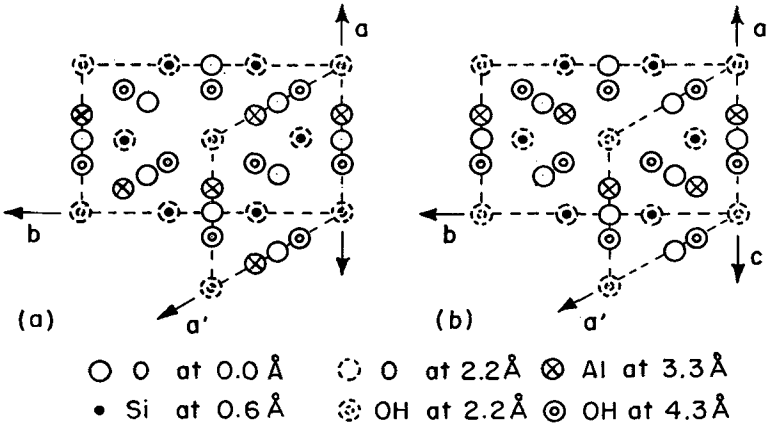

FIG. 9. The structure of (*a*) kaolinite, and (*b*) its mirror image, projected on (001). The α and γ angles of the mirror structure are supplementary to those of kaolinite.

ture (fig. 9*a*) as the correct solution, but its mirror image can be expected to give an identical X-ray diffraction pattern. An anomalous scattering experiment such as that performed on α-quartz by DeVries (1958), and additional physical information (e.g. morphology, etch patterns, or optical activity) would be required to distinguish the enantiomorphic pair. The experiment would be an extremely difficult one since kaolinite crystals are seldom larger than a few microns. Until the absolute configuration is determined it can only be assumed that every specimen of

kaolinite is a mixture of right- and left-handed crystals in unknown proportions. A random interleaving of the two modifications is also possible, in which case the diffraction pattern would show layers randomly displaced by multiples of $b/3$ (cf. table V). Such effects have been observed in English fireclays by Brindley and Robinson (1946*b*).

On the basis of the foregoing arguments concerning Coulomb energy, there is little to differentiate among the twelve two-layer cells of table VII. Secondary variations in the structures occur, however, when the effect of the kaolin-layer distortions on the interlayer bonding is considered. This criterion was first suggested by Brindley and Nakahira (1958) in their study of the triclinic distortions in kaolinite. The irregularities observed in dickite are likely to occur in any kaolin-layer sequence since interatomic forces within a layer are much stronger than those between layers. The most important features affecting the interlayer oxygen–hydroxyl distances are the rotation directions of the silica tetrahedra and the relationship between the pucker of the oxygen network and that of the adjoining hydroxyl sheet. Assuming the rotation directions to be determined by the disposition of aluminium ions, eighteen of the stacking sequences in table VI show longer OH–O contacts while those of the remaining eighteen are strengthened. Unfortunately, however, all twelve of the sequences with minimum cation–cation superposition possess favourable angular rotations. When the puckering of the oxygen and hydroxyl layers is considered, four of the twelve sequences are clearly favoured. As mentioned previously, the buckling of the oxygen layer is caused by the shortened shared edges in the octahedral layer; as a result, the silica tetrahedra are tilted and atom O_3 becomes appreciably higher than O_1 and O_2. The hydroxyl layer also deviates from planarity because $(OH)_3$ shares a short octahedral edge with another hydroxyl group, whereas $(OH)_2$ and $(OH)_4$ are associated with the apex oxygens of the tetrahedral layer. $(OH)_3$ is therefore slightly elevated and the best interlayer linkage is obtained by matching O_3 with $(OH)_3$. The four sequences incorporating these $(OH)_1$–$(OH)_3$–O_3 groups are 11, 20, 27, and 36. Only two of the one- and two-layer unit cells in table VII are composed of the preferred arrangements: 11, 27, 11, 27, 11, . . ., and 20, 36, 20, 36, 20, ... The two-layer structures generated by these sequences are those of dickite and nacrite, respectively. Neither of the kaolinite structures satisfies the pucker criterion; this may explain why kaolinite crystals are seldom as large as those of dickite or nacrite. The crystal structure of nacrite was determined by Hendricks (1938); it is usually characterized as a six-layer pseudo-rhombohedral mineral but

only involves two types of stacking sequences alternating along the *c*-axis. Neither dickite nor nacrite shows enantiomorphism since both belong to the monoclinic point group *m*.

In summary, it has been shown that there are thirty-six stacking sequences which lead to the required interlayer bonding. Twelve of these arrangements are to be preferred if the cation superposition of consecutive layers is minimized. The twelve sequences generate two one-layer unit cells (kaolinite and its mirror image) and twelve two-layer cells (including dickite and nacrite). Unit cells containing more than two kaolin layers were not considered. When the effect of the kaolin layer distortions on the interlayer bonds is considered, the most stable configurations seem to be those of dickite and nacrite.

Acknowledgements. I wish to thank Dr. W. H. Taylor and Prof. A. R. von Hippel for provision of facilities and for their interest and encouragement. Thanks are also due to Messrs. M. Wells and B. Warner for programming the numerical calculations on EDSAC II of the Cambridge Mathematical Laboratory. The infra-red spectrograms were obtained with the assistance of Dr. A. Linz, Jr., and Mr. J. Kalnajs. The dickite specimen was supplied by Prof. G. W. Brindley, who also made several useful comments on the manuscript.

References.

ADLER (H.), BRAY (E. E.), STEVENS (N. P.), HUNT (J. M.), KELLER (W. D.), PICKETT (E. E.), and KERR (P. F.), 1950. Report 8, American Petroleum Institute Project 49, Columbia University, New York.

BATES (T. F.), 1959. Amer. Min., vol. 44, p. 78.

BERGHUIS (J.), HAANAPPEL (IJ.), POTTERS (M.), LOOPSTRA (B. O.), MACGILLAVRY (C. H.), and VEENENDAAL (A. L.), 1955. Acta Cryst., vol. 8, p. 478.

BRINDLEY (G. W.), 1951. X-ray identification and structure of the clay minerals, Min. Soc. Monograph, London, chap. 2.

—— and NAKAHIRA (M.), 1958. Min. Mag., vol. 31, p. 781.

—— and ROBINSON (K.), 1946*a*. Ibid., vol. 27, p. 242.

—— —— 1946*b*. Trans. Faraday Soc., vol. 42B, p. 198.

BUSING (W. R.) and LEVY (H. A.), 1958. Acta Cryst., vol. 11, p. 798.

DEVRIES (A.), 1958. Nature, vol. 181, p. 1193.

FARQUHAR (M. C. M.) and LIPSON (H.), 1946. Proc. Phys. Soc., vol. 58, p. 200.

HENDRICKS (S. B.), 1938. Zeits. Krist., vol. 100, p. 509.

HENRY (N. F. M.), LIPSON (H.), and WOOSTER (W. A.), 1951. The Interpretation of X-ray Diffraction Photographs. London (Macmillan and Co.), p. 161.

HONESS (A. P.) and WILLIAMS (F. J.), 1935. Amer. Min., vol. 20, p. 462.

JOHANNSON (G.), 1959. Acta Cryst., vol. 12, p. 522.

LIPSON (H.) and COCHRAN (W.), 1953. The Determination of Crystal Structures, London (Bell & Sons Ltd.), chap. 9.

MCDONALD (T. R. R.), 1956. Acta Cryst., vol. 9, p. 162.

MEGAW (H. D.), 1934. Zeits. Krist., vol. 87, p. 185.

NAKAMOTO (K.), MARGOSHES (M.), and RUNDLE (R. E.), 1955. Journ. Amer. Chem. Soc., vol. 77, p. 6480.

NEWNHAM (R. E.) and BRINDLEY (G. W.), 1956. Acta Cryst., vol. 9, p. 759; correction: ibid. 1957, vol. 10, p. 88.

SMITH (J. V.), 1954. Acta Cryst., vol. 7, p. 479.

—— and YODER (H. S.), 1956. Min. Mag., vol. 31, p. 209.

WEISZ (O.), COCHRAN (W.), and COLE (W. F.), 1949. Acta Cryst., vol. 2, p. 280.

ZOLTAI (T.) and BUERGER (M. J.), 1959. Zeits. Krist., vol. 111, p. 129.